Available online at www.sciencedirect.com
ScienceDirect
Journal of the European Ceramic Society 31 (2011) 755–762
www.elsevier.com/locate/jeurceramsoc

Effect of step free energy on delayed abnormal grain growth in a liquid phase-sintered $BaTiO_3$ model system

Yoon Ho Heo [a,1], Sang-Chae Jeon [a], John G. Fisher [a,2], Si-Young Choi [b], Kang-Heon Hur [c], Suk-Joong L. Kang [a,*]

[a] *Materials Interface Laboratory, Department of Materials Science and Engineering, Korea Advanced Institute of Science and Technology, Daejeon 305-701, Republic of Korea*
[b] *Korea Institute of Materials Science, Changwon 641-831, Republic of Korea*
[c] *LCR Development Team, Samsung Electro-Mechanics, Suwon 443-743, Republic of Korea*

Received 15 October 2010; accepted 6 December 2010
Available online 8 January 2011

Abstract

The changes in solid/liquid interface structure and grain growth behavior with oxygen partial pressure (P_{O_2}) were systematically studied during liquid-phase sintering of $8TiO_2/2SiO_2$-added $BaTiO_3$. As the P_{O_2} of the sintering atmosphere increased, the grain boundaries and solid/liquid interfaces showed increased faceting, indicating an increase in step free energy. This increase in P_{O_2} and step free energy caused a change in grain growth behavior as a function of sintering time. When samples were sintered in H_2, abnormal grain growth (AGG) occurred from the beginning, resulting in a coarse microstructure with a large average grain size. With increasing P_{O_2}, the incubation time necessary for AGG also increased. Finally, for samples sintered in air, AGG did not occur even after 100 h. These changes in incubation time for abnormal grain growth demonstrate the effect of changing the step free energy on the microstructural development during liquid phase sintering of ceramic systems.

Keywords: Grain growth; Grain boundaries; Interfaces; Microstructure-final, $BaTiO_3$ and titanates

1. Introduction

In $BaTiO_3$, which is a ubiquitously used ceramic in multilayer ceramic capacitors, there have been extensive attempts to predict and control the microstructure through grain boundary engineering. Several studies have focused on how the microstructure varies as the external environment changes, e.g. by changing the kind and concentration of dopant,[1–4] changing the sintering temperature and temperature profile,[5–7] and changing the oxygen partial pressure.[1,8–10] Central to these studies is the structure of the grain boundary or solid/liquid interface, which has been one of the most important parameters in explaining various aspects of microstructural evolution.[11–13] Because grain growth occurs via the movement of grain boundaries or solid/liquid interfaces, to understand the structure and behavior of these boundaries/interfaces is of primary importance.

Previous experiments in several ceramic systems have shown a strong correlation between the structure of the grain boundary or solid/liquid interface and the grain growth behavior.[6,8,10,14–21] Grain boundaries and solid/liquid interfaces can be rough or faceted on an atomic scale. If the boundaries/interfaces are rough, then normal grain growth takes place. If the boundaries/interfaces are faceted, however, different types of normal and abnormal grain growth can occur. The type of grain growth that takes place is determined by the relative values of Δg_{max}, the maximum driving force for grain growth, and Δg_C, the critical driving force for appreciable grain growth.[11–13]

For a system with faceted interfaces, the value of Δg_C, and hence the type of grain growth behavior, can be changed by changing the sintering atmosphere. In the $BaTiO_3$ system, $\{1\,1\,1\}$ twin-assisted abnormal grain growth takes place in samples sintered in air below the eutectic temperature, i.e. in the solid state.[10,22,23] The $\{1\,1\,1\}$ twins form at oxygen partial pressures above $P_{O_2} = 10^{-11}$ atm while $\{1\,1\,1\}$ twins disap-

* Corresponding author. Tel.: +82 42 350 4113; fax: +82 42 350 8920.
E-mail address: sjkang@kaist.ac.kr (S.-J.L. Kang).
[1] Current address: Korea Institute of Science and Technology, 39-1 Hawolgok-dong, Wolsong-gil 5, Seongbuk-gu, Seoul 136-791, Republic of Korea.
[2] Current address: School of Materials Science and Engineering, Chonnam National University, 77 Yongbong-ro, Buk-gu, Gwangju 500-757, Republic of Korea.

0955-2219/$ – see front matter © 2010 Elsevier Ltd. All rights reserved.
doi:10.1016/j.jeurceramsoc.2010.12.010

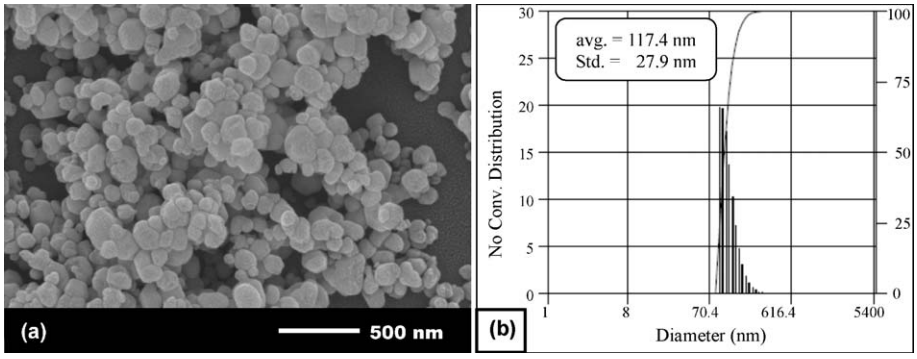

Fig. 1. (a) SEM micrograph of $BaTiO_3$ powder (Sakai Chemical Industry) and (b) its size distribution measured by the dynamic light scattering method.

pear below $P_{O_2} = 10^{-11}$ atm. This changes the grain growth behavior from abnormal with the assistance of {1 1 1} twins ($P_{O_2} = 0.21$ atm) to stagnant without {1 1 1} twins ($P_{O_2} = 10^{-11}$–10^{-17} atm).[10,24] As the sintering atmosphere becomes more reducing, the grain growth behavior changes from stagnant to abnormal (without {1 1 1} twins) then finally to normal.[10] This change of behavior was explained by the reduction of Δg_C in samples sintered in reducing atmospheres.

The above studies show that changes in Δg_C can change the grain growth behavior in solid-state systems, i.e. systems with solid/solid grain boundaries. In contrast, little work has been done to study the effect of Δg_C changes in systems with solid/liquid interfaces. A limited study was carried out by Chang and Kang in the $BaTiO_3$–SiO_2 system.[25] They found that as the sintering atmosphere changed from oxidizing to reducing the grain growth behavior changed from stagnant to abnormal and finally to normal. However, grain growth behavior under only 3 values of P_{O_2} (0.2, $\sim 10^{-17}$ and $\sim 10^{-24}$ atm) was observed and analysis of the solid/liquid interface structure was not carried out. Therefore, to elucidate the effect of changes in Δg_C on the solid/liquid interface structure and grain growth behavior of $BaTiO_3$ in a liquid phase, there is a need for a more detailed study.

A study of grain growth behavior in $BaTiO_3$ with a liquid phase could be done by simply sintering TiO_2-excess $BaTiO_3$ under different oxygen partial pressures at temperatures > 1332 °C (the eutectic temperature of $BaTiO_3$–$Ba_6Ti_{17}O_{40}$ [26]). However, a complicating factor is the formation of abnormal grains of the hexagonal phase of $BaTiO_3$ during sintering in reducing atmospheres at temperatures > 1332 °C.[27,28] It was found that addition of SiO_2 could reduce the eutectic temperature[29] and inhibit the formation of hexagonal $BaTiO_3$.[27] Therefore, in this study $BaTiO_3$ is co-doped with TiO_2 and SiO_2 and sintered in different atmospheres to investigate the effect of oxygen partial pressure on interface structure and grain growth behavior in a system with solid/liquid interfaces without the formation of hexagonal $BaTiO_3$.

2. Experimental

Samples were prepared from $BaTiO_3$ (0.1 μm size and 99.9 wt.% purity, Sakai Chemical Industry, Osaka, Japan), TiO_2 (0.3 μm size and 99.9 wt.% purity, Sigma–Aldrich Co., Milwaukee, WI, USA) and SiO_2 (0.8 μm size and 99.9 wt.% purity, Kojundo Chemical Industry, Saitama, Japan) powders. Fig. 1 shows the SEM micrograph of the $BaTiO_3$ powder (a) and its particle size distribution measured by the dynamic light scattering method (b). The particle sizes are quite uniform with an average value of ~120 nm. A $BaTiO_3$ powder of composition $BaTiO_3$–8 mol.% TiO_2–2 mol.% SiO_2 was prepared. The proportioned powder was ball-milled for 24 h in ethanol in polyethylene bottles using zirconia milling media. After milling, the slurry was dried, crushed and passed through a 150 μm sieve. The powder was lightly pressed into disks with 9 mm diameter and 5 mm thickness, and then compressed isostatically at 200 MPa for 10 min using a Cold Isostatic Press (Autoclave Engineers Inc., Erie, PA, USA). The pressed compacts were pre-annealed at 900 °C for 24 h in order to eliminate volatile impurities. After annealing, samples were placed on $BaTiO_3$ spacers in an alumina crucible and sintered in a closed-end alumina tube in a vertical alumina tube furnace. Samples were sintered at 1280 °C (above the ternary eutectic temperature of 1260 °C for the $BaTiO_3$–SiO_2 pseudo-binary system [29]) for various times up to 100 h. Samples were sintered under different oxygen partial pressures ranging from H_2 ($P_{O_2} = 3.8 \times 10^{-20}$ atm) to air ($P_{O_2} \approx 0.2$ atm). The oxygen partial pressure was controlled using CO/CO_2 and N_2/H_2 mixed gases and measured by a P_{O_2} monitoring system (Nano-Ionics Corporation, Seoul, Korea). Before and after sintering the samples, the closed-end alumina tube was purged with the appropriate mixed gas for 30 min to form the required P_{O_2} value. The sample heating and cooling rate was 10 °C min^{-1}.

Samples for Scanning Electron Microscopy were vertically sectioned, polished and etched in a solution of 1 vol.% HF–4 vol.% HCl–95 vol.% distilled H_2O for 8–10 s. Samples for Scanning Electron Microscopy were gold coated and viewed in an SEM (Model XL 30S FEG, Philips, Eindhoven, The Netherlands). An image analysis program (Matrox Inspector 2.1 Matrox Electronic Systems Ltd., Dorval, Canada) was used to measure the average grain size and grain size distribution of the samples from the micrographs. For each sintering condition, more than 300 grains were examined.

For Transmission Electron Microscopy, samples were ultrasonically cut into 3 mm discs, mechanically ground to a thickness of 100 μm, dimpled to a thickness of less than 10 μm,

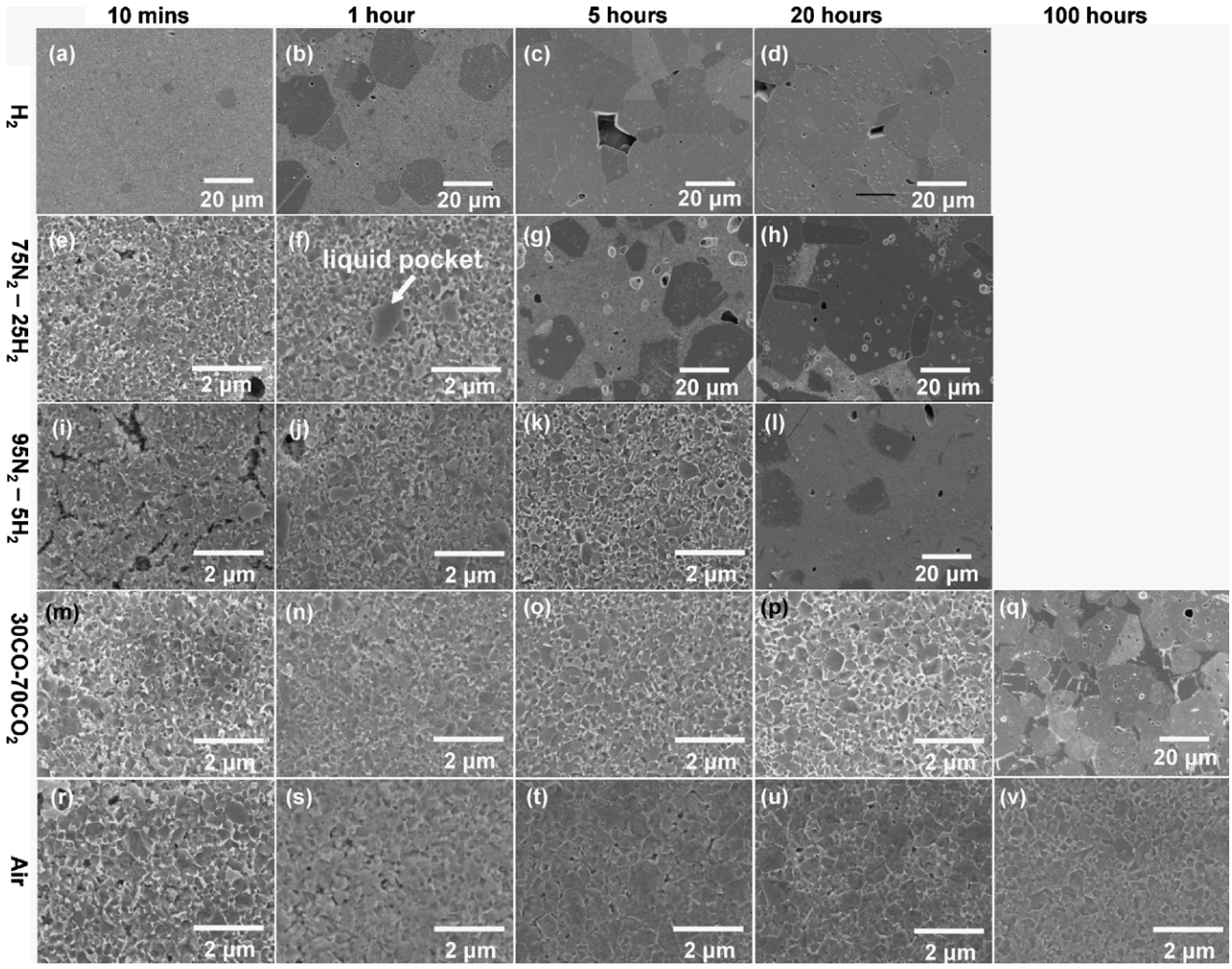

Fig. 2. SEM micrographs of 8 mol.%–TiO_2/2 mol.%–SiO_2 added $BaTiO_3$ sintered at 1280 °C for various times in: (a–d) H_2 ($P_{O_2} = 3.8 \times 10^{-20}$ atm); (e–h) $75N_2$–$25H_2$ (4.1×10^{-18} atm); (i–l) $95N_2$–$5H_2$ (6.3×10^{-16} atm); (m–q) 30CO–70CO_2 (4.6×10^{-10} atm); (r–v) air (2.1×10^{-1} atm).

and finally ion-milled until perforation for electron transparency. High Resolution TEM (HRTEM) observations were performed using two kinds of TEM (Tecnai G2 F30, FEI & Philips CM20, Eindhoven, The Netherlands) operated at 200 and 300 kV, respectively.

3. Results

Fig. 2 shows the microstructures of 8TiO_2/2SiO_2 added $BaTiO_3$ samples which were sintered at 1280 °C for various times from 10 min to 100 h in atmospheres ranging from H_2 ($P_{O_2} = 3.8 \times 10^{-20}$ atm) to air ($P_{O_2} \approx 0.2$ atm). To save space, not all of the microstructures are shown in Fig. 2; however, the grain size distributions of all the samples are given in Fig. 3. Fig. 2(a)–(d) shows the microstructures of the samples which were sintered in H_2 ($P_{O_2} = 3.8 \times 10^{-20}$ atm) and Fig. 3(a) shows the corresponding grain size distributions. For the case of 0 min of sintering, the average grain size was approximately 0.2 μm, abnormal grains were not present and the grain size distribution was unimodal as shown in Fig. 3(a). After 10 min of sintering, a few large (abnormal) grains had already formed [Fig. 2(a)]. After 1 h, the size of abnormal grains increased and their number also increased [Fig. 2(b)]. As the sintering time increased, the number and size of the abnormal grains further increased. Finally, the fine matrix grains were completely consumed by abnormal grains at a sintering time of 5 h and the grain size distribution became unimodal again [Figs. 2(c) and 3(a)]. After that, the average grain size increased slightly, maintaining a unimodal grain size distribution until 50 h [Fig. 3(a)]. None of the abnormal grains contained any {1 1 1} twins.

In the less reducing atmosphere of $75N_2$–$25H_2$ ($P_{O_2} = 4.1 \times 10^{-18}$ atm), the grain growth behavior was different from that above. Fig. 2(e)–(h) shows the microstructures of 8TiO_2/2SiO_2 added $BaTiO_3$ which was sintered at 1280 °C from 0 min to 20 h in $75N_2$–$25H_2$ ($P_{O_2} = 4.1 \times 10^{-18}$ atm), and Fig. 3(b) shows the corresponding grain size distributions for samples sintered for up to 50 h. Until 2 h, the unimodal grain size distribution was maintained as shown in Figs. 2(e)–(f) and 3(b). However, the average grain size increased slightly, which was confirmed by the shift to larger sizes of the grain size distributions [Fig. 3(b)]. Between 2 h and 5 h, abnormal grains appeared (Figs. 2(f) and 3(b)) and as a result of that, the grain size dis-

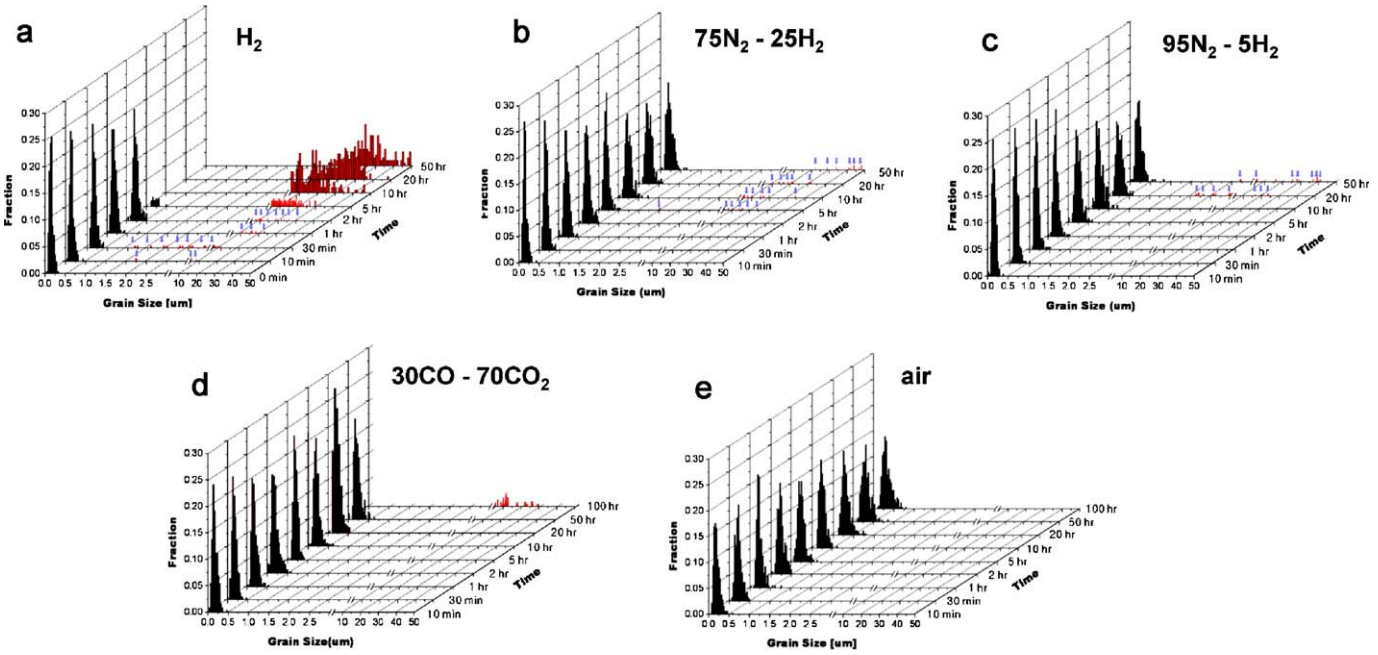

Fig. 3. Grain size distributions of 8 mol.%–TiO_2/2 mol.%–SiO_2 added $BaTiO_3$ sintered at 1280 °C for times from 0 min up to 100 h in: (a) H_2 ($P_{O_2} = 3.8 \times 10^{-20}$ atm); (b) $75N_2$–$25H_2$ (4.1×10^{-18} atm); (c) $95N_2$–$5H_2$ (6.3×10^{-16} atm); (d) 30CO–$70CO_2$ (4.6×10^{-10} atm); (e) air (2.1×10^{-1} atm).

tribution became bimodal. With increasing sintering time, the abnormal grains grew as shown in Fig. 2(h). The matrix grains also grew, but at a very slow rate [Fig. 3(b)]. In the micrographs taken at higher magnification, a TiO_2/SiO_2-containing second phase can be seen [e.g. that indicated by an arrow in Fig. 2(f)]. This phase was present in all samples regardless of sintering atmosphere.

Fig. 2(i)–(l) shows the microstructures of $8TiO_2$/$2SiO_2$ added $BaTiO_3$ which was sintered at 1280 °C for 10 min to 20 h in $95N_2$–$5H_2$ ($P_{O_2} = 6.3 \times 10^{-16}$ atm), and Fig. 3(c) shows the grain size distributions for samples sintered from 10 min to 50 h. For the samples sintered in $95N_2$–$5H_2$, the incubation time for abnormal grain growth became longer than in the cases of sintering in H_2 and $75N_2$–$25H_2$. For sintering times up to 10 h, no abnormal grains appeared. Matrix grain growth was also limited [Fig. 3(c)]. After sintering for 20 h, abnormal grains appeared [Fig. 2(l)]. With further sintering, the size of the abnormal grains increased but the size distribution of the fine matrix grains did not change noticeably [Fig. 3(c)].

Fig. 2(m)–(q) shows the microstructures of $8TiO_2$/$2SiO_2$ added $BaTiO_3$ which was sintered at 1280 °C from 10 min to 100 h in 30CO–$70CO_2$ ($P_{O_2} = 4.6 \times 10^{-10}$ atm) and Fig. 3(d) shows the corresponding grain size distributions. After 10 min of sintering, the average grain size was approximately 0.2 μm, and a unimodal grain size distribution appeared as shown in Figs. 2(m) and 3(d). The unimodal grain size distribution was maintained up to 50 h and abnormal grains did not appear. Between 50 and 100 h, abnormal grains appeared and by 100 h of sintering the fine sized matrix grains were completely consumed by large abnormal grains of size 5–30 μm [Figs. 2(q) and 3(d)].

Finally, in air ($P_{O_2} \approx 2.1 \times 10^{-1}$ atm), abnormal grains did not appear even after sintering for 100 h, as shown in Fig. 2(r)–(v). From 10 min to 100 h, the only change with increasing sintering time was the broadening of the grain size distributions [Fig. 3(e)]. When all the results are considered, it can be seen that the incubation time necessary for AGG increased with increasing P_{O_2}. The incubation time for AGG gradually increased from a few min to more than 100 h as P_{O_2} increased from $\sim 10^{-20}$ atm to $\sim 10^{-1}$ atm.

Fig. 4 shows the typical morphologies of grain boundaries under different values of P_{O_2}. Microfaceted boundaries with a hill-and-valley shape are marked with arrows. Only a small fraction of the boundaries appear faceted in the sample sintered in H_2 ($P_{O_2} = 3.8 \times 10^{-20}$ atm) [Fig. 4(a)]. The fraction of faceted boundaries increases as P_{O_2} increases to 2.1×10^{-1} atm [Figs. 4(b) and (c)], implying that the boundary step free energy increases with increasing P_{O_2}. High resolution TEM (HRTEM) observation revealed that the grain boundaries were free of an amorphous phase, for example, as shown in Fig. 4(d).

The change in morphology of the solid/liquid interface with oxygen partial pressure was identified by observing the shape of entrapped liquid drops within grains. The shape of an entrapped liquid drop (a negative crystal) exhibits the equilibrium shape of a crystal in the same liquid.[30,31] Many entrapped liquid drops were present in some regions of several grains, as shown in Fig. 5. (An EDS analysis revealed the average concentration of Si in three pockets to be 33.4 at.% in H_2, and 35.5 at.% in air, demonstrating that the pockets are liquid drops rather than entrapped pores.) The shapes of liquid drops in samples annealed in H_2 (Fig. 5(a)) are mostly rounded with a small fraction of facets. Fig. 5(b) is an HRTEM micrograph of a small liquid drop. The solid/liquid interface appears to be mostly defecated except at a (0 0 1) plane, which is apparently flat. In contrast, Fig. 5(c) shows that the shape of entrapped liquid drops is mostly well faceted in

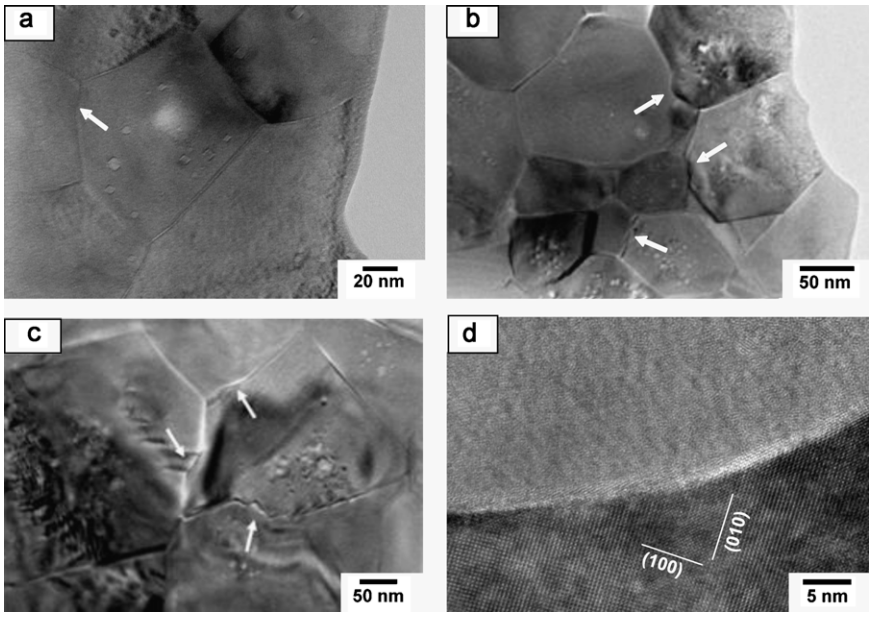

Fig. 4. TEM images of grain boundary morphology of 8 mol.%–TiO_2/2 mol.%–SiO_2 added $BaTiO_3$ sintered at 1280 °C for 30 min in: (a) and (d) H_2 (3.8×10^{-20} atm), (b) 30CO/70CO_2 (4.6×10^{-10} atm), and (c) air (2.1×10^{-1} atm). Faceted boundaries with a hill-and-valley shape, are indicated by arrows.

air. The HRTEM micrograph in Fig. 5(d) shows faceted {0 0 1} planes and also faceted {1 1 1} planes. These TEM observations demonstrate an increase in the step free energy of solid/liquid interfaces with an increasing oxygen partial pressure.

4. Discussion

The SEM and TEM results in the present work show that the SiO_2/TiO_2 liquid phase remains at multi-grain junctions and does not penetrate the grain boundaries (Figs. 2 and 4). Even in this case, the grain growth behavior may be controlled by a solution–reprecipitation process through the liquid phase at the multi-grain junctions.[32] In the following explanation of the grain growth behavior, it will be assumed that grain growth takes place via such a process because the distance of material transport is larger at triple junctions than at grain boundaries. A similar explanation could, however, also be made if grain growth takes place via atomic diffusion across the solid–solid grain boundaries.[10,33,34]

Solid/liquid interfaces can have two structures: atomically rough or atomically smooth (faceted).[35–37] On a microscopic scale, atomically rough interfaces will appear curved whereas

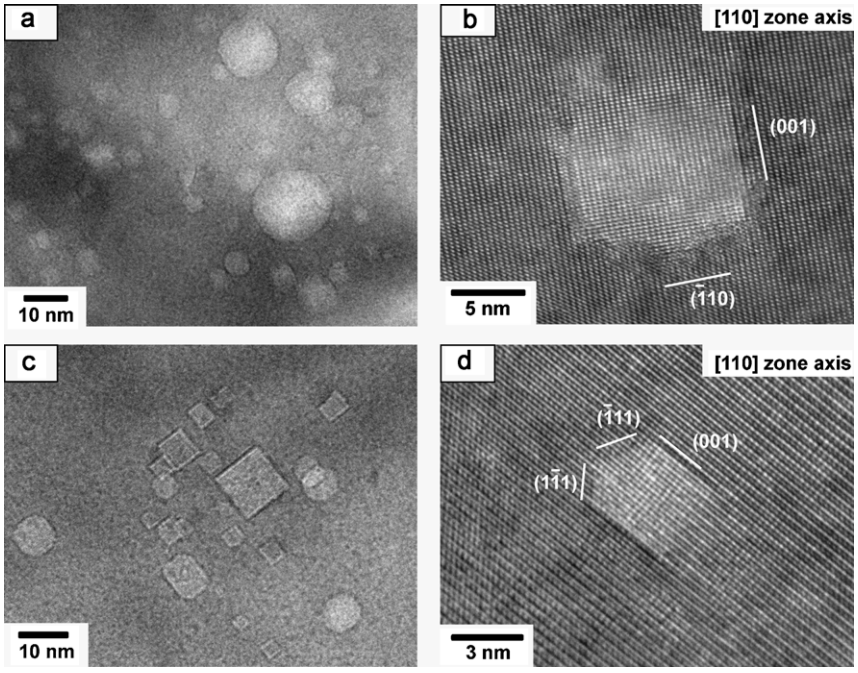

Fig. 5. TEM and HRTEM micrographs showing the shapes of liquid drops entrapped within $BaTiO_3$ grains (a) and (b) in H_2, and (c) and (d) in air.

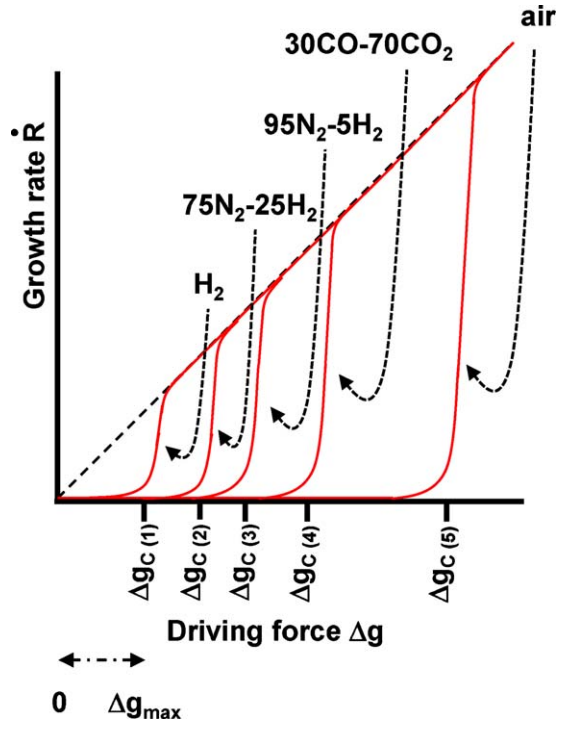

Fig. 6. Schematic showing the difference in critical driving force (Δg_C) among the samples that were sintered in variable P_{O_2}. (The maximum driving force for grain growth at initial time of sintering is also expressed.)

atomically smooth interfaces will be flat, often with a hill and valley or microfaceted appearance. During grain growth, atoms must cross the solid/liquid interface between the growing and shrinking grain and then attach to the growing grain. If the interface is atomically rough, then there are a large number of kink sites on the growing grain to which atoms can attach. The grain growth rate is therefore controlled by the rate of diffusion across the interface. If the interface is atomically smooth, however, then the number of kink sites on the growing grain will be limited. In order to grow, the grain must possess kink sources such as 2D nuclei or screw dislocations.[37] The grain growth is then controlled by the rate at which atoms can attach to the kink sources. Solid/liquid interface migration by the lateral movement of steps on a growing crystal has been well documented in the literature.[36,38]

Fig. 6 plots schematically the variation in growth rate with driving force for a grain with atomically rough or atomically smooth interfaces. For both cases, the driving force for grain growth is due to the difference in solubility between large and small grains (Ostwald ripening). The driving force Δg for grain growth is given by[12,39]:

$$\Delta g = 2\gamma V_m \left(\frac{1}{\bar{r}} - \frac{1}{r}\right) \quad (1)$$

where γ is the solid/liquid interfacial energy, V_m is the molar volume of the solid phase, and $\bar{r}$ is the radius (in the case of faceted grains, the distance from the center to the facet plane) of a grain which is neither growing nor shrinking. For an atomically rough interface, the grain growth rate is a linear function of the driving force.[40] In diffusion-controlled growth, any grain with a positive driving force Δg can grow. Upon extended sintering, the grain size distribution will become stationary with a maximum value approximately twice that of the mean grain size.[40] In particular, abnormal grain growth will not occur.

For an atomically smooth interface in which growth is controlled, in many cases, by 2D nucleation, the grain growth rate can be given by[34,37]:

$$\frac{dr}{dt} = hA\Psi n_0 \exp\left(-\frac{\pi\varepsilon^2}{kTh\Delta g}\right) \quad (2)$$

where $\Psi = n^* \upsilon \exp\left(-\frac{\Delta g_m}{kT}\right)$, υ is the vibration frequency of atoms in the liquid, n^* the number of atoms in a position close to the nucleus, Δg_m the activation energy for jumping across the interface, A the grain facet area, n_0 the number density of atoms in the liquid, h the height of the 2D nucleus, ε the step free energy of the nucleus, k the Boltzmann constant, T the absolute temperature, and Δg the driving force for grain growth, as given in Eq. (1). In 2D nucleation-controlled growth, the grain growth rate is an exponential function of the driving force. The growth rate will be very low until a critical driving force Δg_C is reached, at which point it increases drastically with driving force. At $\Delta g > \Delta g_C$, kinetic roughening takes place and the interface can effectively become atomically rough.[41] From this point, the grain growth rate is controlled by diffusion and the growth rate increases linearly with Δg (Fig. 6). The value of the critical driving force Δg_C is given by[42]:

$$\Delta g_C = \frac{V_m \varepsilon^2}{3hkT} \quad (3)$$

From Eqs. (2) and (3), it can be seen that the grain growth behavior of a polycrystalline material is strongly affected by the step free energy ε. This is the excess energy associated with the edge of the 2D nucleus and is analogous with the step energy of a vicinal surface. Theoretical calculations indicate that as the step free energy changes the grain growth behavior also changes.[12,39] With increasing step free energy, the grain growth behavior can change from pseudo-normal to abnormal to time-delayed abnormal to stagnant.[12]

The value of the step free energy ε can be varied by dopant addition,[43] changing temperature[44] and changing sintering atmosphere. The step energy is inversely related to the configurational entropy,[44,45] which can be increased by the creation of vacancies.[46] Indeed, previous experiments with $SrTiO_3$ and $BaTiO_3$ have shown that sintering in reducing atmospheres induces a roughening transition at the grain boundaries and a change in grain growth behavior from abnormal to normal.[10,15] This is caused by the increased oxygen vacancy concentration in the samples sintered in reducing atmospheres. In the present work, the increase in microfaceting with increase in P_{O_2} (Fig. 4) and the shape change of liquid drops from mostly rounded to faceted (Fig. 5) indicate that the step free energy ε is increasing with increasing P_{O_2}.[10]

The grain growth behavior in the $8TiO_2/2SiO_2$ added $BaTiO_3$ samples sintered in different atmospheres can be explained as follows: at the start of sintering, the grains in each sample will have a range of driving forces for growth as determined by the

size distribution of the starting powder. The largest grain will have a driving force Δg_{max}. As all the samples were prepared from the same batch of powder, the value of Δg_{max} for all samples should be approximately equal. The samples sintered in H_2 ($P_{O_2} = 3.8 \times 10^{-20}$ atm) have the highest vacancy concentration because of extensive formation of oxygen vacancies in a highly reducing atmosphere[47] and hence the lowest values of ε and Δg_C (Δg_{C1} in Fig. 6). Most of the grains have $\Delta g < \Delta g_C$, and only a few large grains may have $\Delta g > \Delta g_C$ and can grow rapidly to form abnormal grains [Fig. 2(a) and (b)]. When these abnormally growing grains impinge upon each other, their growth rate will decrease rapidly [Figs. 2(c) and (d), and 3(a)]. This type of abnormal grain growth behavior in pure H_2 is different from the previous results of Chang and Kang[25] where pseudo-normal grain growth was observed in $90BaTiO_3$–$10SiO_2$ sintered in H_2. The difference in growth behavior between the two investigations must be due to the difference in chemical composition of the liquid phase. It appears that excess TiO_2 increases the step free energy. In fact, addition of excess TiO_2 is known to promote abnormal grain growth in solid state-sintered $BaTiO_3$.[23,48] The difference in oxygen partial pressure between the two H_2 atmospheres could also affect the growth behavior.

For the samples sintered in $75N_2$–$25H_2$ the total vacancy concentration in the samples is expected to decrease. This causes an increase in ε and Δg_C (Δg_{C2} in Fig. 6). Now all of the grains have $\Delta g < \Delta g_C$ and so the grain growth is very slow [Figs.1(e) and (f), and 3(b)]. Nevertheless, the growth rate, even though it is low, increases with increasing grain size because the growth rate is an exponential function of the driving force. This can result in an increase in the driving force of the largest grain so that it has a value larger than Δg_C.[12] Therefore some large grains can grow abnormally after a certain period of time, as observed in the sample sintered for 5 h in $75N_2$–$5H_2$ [Figs. 2(g) and 3(b)]. The grain growth behavior has changed from abnormal in H_2 to time-delayed abnormal in $75N_2$–$25H_2$. Note that the number of abnormal grains in this case is lower than in the samples sintered in H_2 and that the majority of grains are small matrix grains, even after 50 h.

As the sintering atmosphere becomes progressively more oxidizing, the total vacancy concentration in the samples continues to decrease and ε and Δg_C continue to increase in value (Δg_{C3} and Δg_{C4} in Fig. 6). This increases the incubation time needed for grains to grow large enough to have values of $\Delta g > \Delta g_C$ and hence to grow rapidly to form abnormal grains [Figs. 2(l) and (q), and 3(c) and (d)]. Eventually, for the samples sintered in air, Δg_C is so large (Δg_{C5} in Fig. 6) that none of the grains grow large enough to have values of $\Delta g > \Delta g_C$ even after 100 h of sintering [Figs. 2(v) and 3(e)]. The grain growth behavior has changed from time-delayed abnormal to stagnant.

The above results show the step free energy-dependent grain growth behavior in the TiO_2/SiO_2 added $BaTiO_3$ system. The observed grain growth behavior can be well explained by the change in critical driving force Δg_C with P_{O_2} and the change in maximum driving force Δg_{max} with grain growth of matrix grains. The present results may further demonstrate the possibility of microstructure control, either fine, duplex, or course-grained, of ceramics by controlling the values of ε and Δg_C via control of the sintering atmosphere.

5. Conclusions

The correlation between grain growth behavior, step free energy ε, and P_{O_2} has been investigated systematically for the first time in a liquid phase sintered system of 8 mol.% TiO_2/2 mol.% SiO_2 added $BaTiO_3$. By systematically changing P_{O_2} from 3.8×10^{-20} atm to 0.21 atm, we observed the microstructures and measured grain size distributions according to the sintering time. At $P_{O_2} = 3.8 \times 10^{-20}$ atm (H_2), where the value of the critical driving force for grain growth Δg_C was relatively low, AGG occurred from the beginning of sintering. As P_{O_2} increased, both the step free energy ε and the critical driving force for grain growth Δg_C increased. This resulted in an increase in the incubation time for abnormal grain growth. At ($75N_2$–$25H_2$), AGG occurred in 5 h whereas abnormal grains appeared in 20 h in the case of $P_{O_2} = 6.3 \times 10^{-16}$ atm ($95N_2$–$5H_2$). In a more oxidizing atmosphere at ($30CO$–$70CO_2$), AGG occurred between 50 and 100 h and finally, AGG did not occur even after 100 h of sintering at $P_{O_2} = 0.21$ atm (air).

For the same initial particle size distribution, the incubation time is dependent on the step free energy which varies with oxygen partial pressure. TEM results show that the grain boundary and solid/liquid interface faceting gradually increase with increasing P_{O_2}, indicating an increase in step free energy ε. As ε increases, the critical driving force for grain growth increases which changes the time dependent grain growth behavior from abnormal to time-delayed abnormal and finally to stagnant. The difference in incubation time for AGG can be explained in terms of the variation of the interface structure and the critical driving force for appreciable growth with respect to oxygen partial pressure. These results show that the relationship between P_{O_2}, step free energy ε, interface structure, and grain growth behavior in solid-state systems can be extended to liquid phase sintered systems.

Acknowledgments

This work was supported by the National Research Foundation of Korea (NRF) (Grant No. 2009-0094039) funded by the Ministry of Education, Science and Technology, Korea, and also the Center for Advanced MLCC Manufacturing Processes funded by Samsung Electro-Mechanics Co.

References

1. Shimsnskij AF, Drofenik M, Kolar D. Subsolidus grain growth in donor doped barium titanate. *J Mater Sci* 1994;**29**:6301–5.
2. Lin MH, Chou JF, Lu HY. Grain-growth inhibition in Na_2O-doped TiO_2-excess barium titanate ceramic. *J Am Ceram Soc* 2000;**83**:2155–62.
3. Drofenik M, Makovec M, Zajc I, Langhammer HT. Anomalous grain growth in donor-doped barium titanate with excess barium oxide. *J Am Ceram Soc* 2002;**85**:653–60.
4. Fisher JG, Choi SY, Kang SJL. Abnormal grain growth in barium titanate doped with alumina. *J Am Ceram Soc* 2006;**89**:2206–12.

5. Kang MG, Kim DY, Lee HY, Hwang NM. Temperature dependence of the coarsening behavior of barium titanate ceramics. *J Am Ceram Soc* 2000;**83**:3202–4.
6. Kang MK, Park JK, Kim DY, Hwang NM. Effect of temperature on the shape and coarsening behavior of $BaTiO_3$ grains dispersed in a SiO_2-rich liquid matrix. *Mater Lett* 2000;**45**:43–6.
7. Wang XH, Deng XY, Bai HL, Zhou H, Qu WG, Li LT, et al. Two-step sintering of ceramics with constant grain-size. II: $BaTiO_3$ and Ni–Cu–Zn ferrite. *J Am Ceram Soc* 2006;**89**:438–43.
8. Lee BK, Chung SY, Kang SJL. Grain boundary faceting and abnormal grain growth in $BaTiO_3$. *Acta Mater* 2000;**48**:1575.
9. Choi SY, Kang SJL. Sintering kinetics by structural transition at grain boundaries in barium titanate. *Acta Mater* 2004;**52**:2937–43.
10. Jung YI, Choi SY, Kang SJL. Effect of oxygen partial pressure on grain boundary structure and grain growth behavior in $BaTiO_3$. *Acta Mater* 2006;**54**:2849–55.
11. Jo W, Kim DY, Hwang NM. Effect of interface structure on the microstructural evolution of ceramics. *J Am Ceram Soc* 2006;**89**:2369–80.
12. Jung YI, Yoon DY, Kang SJL. Coarsening of polyhedral grains in a liquid matrix. *J Mater Res* 2009;**24**:2949–59.
13. Kang SJL, Lee MG, An SM. Microstructural evolution during sintering with control of the interface structure. *J Am Ceram Soc* 2009;**92**:1464–71.
14. Kwon SK, Hong SH, Kim DY, Hwang NM. Coarsening behavior of tricalcium silicate (C_3S) and dicalcium silicate (C_2S) grains dispersed in a clinker melt. *J Am Ceram Soc* 2000;**83**:1247–52.
15. Chung SY, Yoon DY, Kang SJL. Effects of donor concentration and oxygen partial pressure on interface morphology and grain growth behavior in $SrTiO_3$. *Acta Mater* 2002;**50**:3361–71.
16. Park CW, Yoon DY. Abnormal grain growth in alumina with anorthite liquid and the effect of MgO addition. *J Am Ceram Soc* 2002;**85**:1585–93.
17. Jang CW, Kim J, Kang SJL. Effect of sintering atmosphere on grain shape and grain growth in liquid-phase-sintered silicon carbide. *J Am Ceram Soc* 2002;**85**:1281–4.
18. King PT, Gorzkowski EP, Scotch AM, Rockosi DJ, Chan HM, Harmer MP. Kinetics of $\{0\,0\,1\}$ $Pb(Mg_{1/3}Nb_{2/3})O_3$–35 mol.% $PbTiO_3$ single crystals grown by seeded polycrystal conversion. *J Am Ceram Soc* 2003;**86**:2182–7.
19. Cho YK, Yoon DY, Kim BK. Surface roughening transition and coarsening of NbC grains in liquid cobalt-rich matrix. *J Am Ceram Soc* 2004;**87**:443–8.
20. Yoon BK, Lee BA, Kang SJL. Growth behavior of rounded (Ti, W)C and faceted WC grains in a Co matrix during liquid phase sintering. *Acta Mater* 2005;**53**:4677–85.
21. Fisher JG, Kang SJL. Microstructural changes in $(K_{0.5}Na_{0.5})NbO_3$ ceramics sintered in various atmospheres. *J Eur Ceram Soc* 2009;**29**:2581–8.
22. DeVries RC. Observations on growth of $BaTiO_3$ crystals from KF solutions. *J Am Ceram Soc* 1959;**42**:547–58.
23. Lee BK, Kang SJL. Second-phase assisted formation of $\{1\,1\,1\}$ twins in barium titanate. *Acta Mater* 2001;**49**:1373–81.
24. Jung YI, Lee BK, Kang SJL. Effect of $Ba_6Ti_{17}O_{40}/BaTiO_3$ interface structure on $\{1\,1\,1\}$ twin formation and abnormal grain growth in $BaTiO_3$. *J Am Ceram Soc* 2004;**87**:739–41.
25. Chang J, Kang SJL. Step free energy change and microstructural development in $BaTiO_3$–SiO_2. *Key Eng Mater* 2007;**352**:25–30.
26. Kirby KW, Wechsler BA. Phase relations in the barium titanate–titanium oxide system. *J Am Ceram Soc* 1991;**74**:1841–7.
27. Glaister RM, Kay HF. An investigation of the cubic-hexagonal transition in barium titanate. *Proc Phys Soc* 1960;**76**:763–72.
28. Rečnik A, Kolar D. Exaggerated growth of hexagonal barium titanate under reducing sintering conditions. *J Am Ceram Soc* 1996;**79**:1015–8.
29. Rase DE, Roy R. Phase equilibria in the system $BaTiO_3$–SiO_2. *J Am Ceram Soc* 1955;**38**:389–95.
30. Miller WA, Chadwick GA. The equilibrium shapes of small liquid droplets in solid–liquid phase mixtures: metallic h.c.p. and metalloid systems. *Proc Roy Soc Ser A* 1969;**312**:257–76.
31. Park SY, Choi K, Kang SJK, Yoon DN. Shape of $MgAl_2O_4$ grains in a CaMgSiAlO glass matrix. *J Am Ceram Soc* 1992;**75**:216–9.
32. Kang SS, Yoon DN. Kinetics of grain coarsening during sintering of Co–Cu and Fe–Cu alloys with low liquid contents. *Metall Trans A* 1982;**13**:1405–11.
33. Jung YI, Choi SY, Kang SJL. Grain-growth behavior during stepwise sintering of barium titanate in hydrogen has and air. *J Am Ceram Soc* 2003;**86**:2228–30.
34. Yoon DY, Park CW, Koo JB. The step growth hypothesis for abnormal grain growth. In: Kang SJL, editor. *Ceramic Interfaces*, vol. 2. London: Institute of Materials; 2001. p. 3–21.
35. Yamamoto T, Ikuhara Y, Watanabe T, Sakuma T, Taniuchi Y, Okada K, et al. High resolution microscopy study in Cr_3C_2-doped WC–Co. *J Mater Sci* 2001;**36**:3885–90.
36. Wolf PE, Gallet F, Balibar S, Rolley E. Crystal growth and crystal curvature near roughening transitions in hcp ^{4}He. *J Phys* 1985;**46**:1987–2009.
37. Hirth JP, Pound GM. *Condensation and Evaporation: Nucleation and Growth Kinetics*. Oxford: Pergamon Press; 1963. pp. 77–148.
38. Malkin AJ, Kuznetsov YG, McPherson A. In situ atomic force microscopy studies of surface morphology, growth kinetics, defect structure and dissolution in macromolecular crystallization. *J Cryst Growth* 1999;**196**:471–88.
39. Kang SJL. *Sintering: Densification, Grain Growth & Microstructure*. Amsterdam: Elsevier; 2005. pp. 205–220.
40. Ardell AJ. The effect of volume fraction on particle coarsening: theoretical considerations. *Acta Metall* 1972;**20**:61–71.
41. Peteves SD, Abbaschian R. Growth kinetics of solid–liquid Ga interfaces: Part II. *Theor Metall Trans A* 1991;**22**:1271–86.
42. van der Erden JP. Crystal growth mechanisms. In: Hurle DTJ, editor. *Handbook of Crystal Growth vol. 1,Fundamentals Part A, Thermodynamics and Kinetics*. Amsterdam: Elsevier Science Publishers; 1993. p. 311–475.
43. Givargizov EI. *Oriented Crystallization on Amorphous Substrates*. New York: Plenum Press; 1991. pp. 1–62.
44. Williams ED. Surface steps and surface morphology: understanding macroscopic phenomena from atomic observations. *Surf Sci* 1994;**299/300**:502–24.
45. Burton WK, Cabrera N, Frank FC. The growth of crystals and the equilibrium structure of their surfaces. *Philos Trans R Soc Lon Ser A* 1951;**243**:299–358.
46. Chiang YM, Birnie III D, Kingery WD. *Physical ceramics: principles for ceramic science and engineering*. New York: John Wiley & Sons; 1997. pp. 101–84.
47. Lee HS, Mizoguchi T, Yamamoto T, Kang SJL, Ikuhara Y. First-principles calculation of defect energetic in cubic-$BaTiO_3$ and a comparison with $SrTiO_3$. *Acta Mater* 2007;**55**:6535–40.
48. Lee BK, Chung SY, Kang SJL. Necessary conditions for the formation of $\{1\,1\,1\}$ twins in barium titanate. *J Am Ceram Soc* 2000;**83**:2858–60.